

# Emulating a broadband frequency sweep for Terahertz thin-film imaging

Amlan kusum Mukherjee and Sascha Preu  
Technische Universität Darmstadt, Darmstadt, 64283, HE, Germany

**Abstract**—Conventional continuous-wave Terahertz imaging and thickness resolution systems often rely on the Fabry-Pérot resonances generated in the sample being imaged. As the samples become thinner, larger frequency sweeps are necessary for their visualisation. In this work, we demonstrate a post-processing technique employing zero-padding of a smaller frequency sweep between frequency intervals as low as 10 GHz up to intervals of 200 GHz, conducted between 0.6-0.8 THz, to emulate the thickness resolution generally achieved by orders of magnitude larger frequency ranges.

©2022 IEEE. Published version:  
<https://ieeexplore.ieee.org/document/9895797>

## I. INTRODUCTION

Terahertz (THz) imaging can be used in a plethora of applications in diverse domains like security, biomedicine, material analysis, etc [1]. Recently, we demonstrated nanometric imaging capabilities with a precision of only 28 nm from a continuous-wave (CW) frequency scan conducted between 0.6 – 0.8 THz [2]. This technique, as well as other conventional thickness measurement algorithms, relies on the Fabry-Pérot oscillations generated in a relatively thick host wafer, attached to these thin structures to be imaged. Generally, the phase change induced by the Fabry-Pérot resonances in transmitted Terahertz waves ( $\Phi_T$ ) through a sample of optical thickness  $d_{opt}$  is given by [3],

$$\Phi_T = \tan^{-1} \left[ \frac{R+1}{R-1} \tan \left( 2\pi \frac{d_{opt}}{\lambda} \right) \right], \quad (1)$$

where  $R$  is the power reflection coefficient and  $\lambda$  is the scanning wavelength. For thin samples and small measurement intervals  $d_{opt}/\lambda \rightarrow 0$ , the Fabry-Pérot features eventually vanish,  $\Phi_T$  increases only linearly with frequency. Evaluating the Fabry-Pérot oscillations becomes thus extremely difficult and necessitates scanning bandwidths in the order of a few Terahertz or more in order to capture at least one Fabry-Pérot period [4]. In this work, we emulate such a high bandwidth frequency sweep by a scan as short as 200 GHz conducted between 0.6 – 0.8 THz. We first image a 10  $\mu\text{m}$  deep Siemens star etched into a 520  $\mu\text{m}$  thick highly-resistive silicon (HR-Si) wafer. We further extend our methodology to image nanometric silicon nitride depositions on HR-Si and finally, to a 40  $\mu\text{m}$  thick lossy polyvinylchloride based adhesive tape.

Fig. 1 shows a schematic of the CW measurement setup. We use a PIN-diode based commercial transmitter manufactured by Toptica Photonics/Fraunhofer HHI as THz source. A parabolic mirror is placed after the source to collect and collimate the emitted divergent THz beam onto the TPX lens placed before the sample under test. The sample is mounted on a two-dimensional motorised stage for conducting single-pixel raster scan and is placed between two Polymethylpentene (TPX) lenses which focuses the THz beam on to the sample. The radius of the THz beam spot on the sample is  $\approx 550 \mu\text{m}$  at 800 GHz.

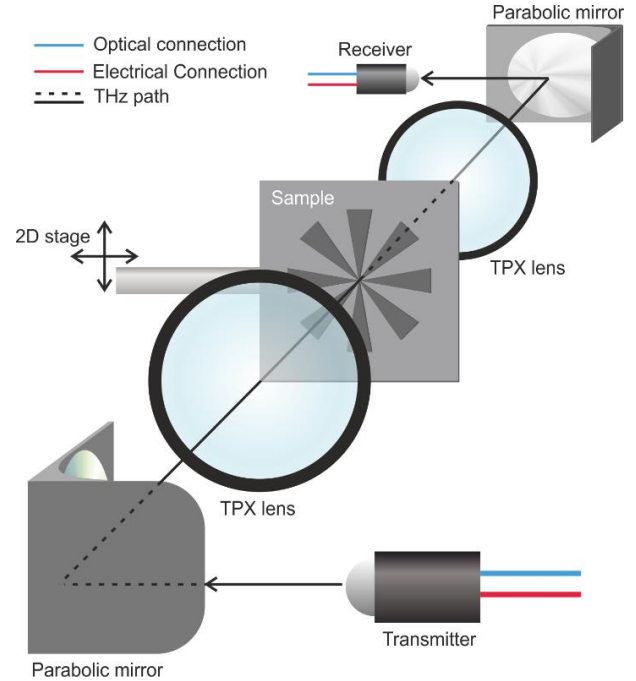
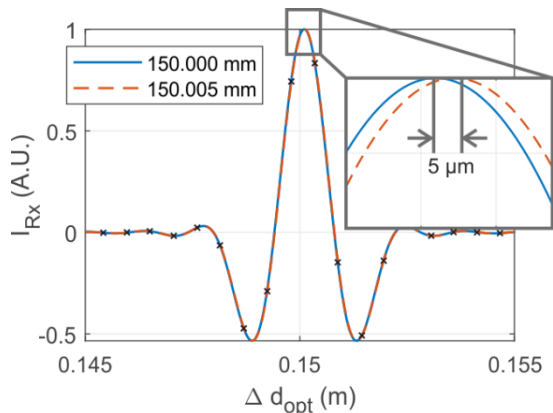


Fig. 1. Schematic of the measurement setup.

Another parabolic mirror is used to refocus the transmitted beam onto an ErAs:In(AI)GaAs based receiver developed in-house [5] or, alternatively, a commercial photoconductive receiver. Both the transmitter and the receiver are driven by the same set of distributed feedback (DFB) lasers with a difference frequency of the desired terahertz frequency. The output current of the receiver is subsequently amplified using a low-noise transimpedance amplifier (PDA-S, TEM Messtechnik), with a transimpedance of  $10^6 \text{ V/A}$ , before being fed to a commercial lock-in amplifier for demodulation. The setup is operated in a homodyne fashion and frequency sweeps are carried out between 0.6 – 0.8 THz for each position of the raster scan, referred henceforth as pixels, with a frequency resolution of 50 MHz. The pixels are separated from each other by 0.5 mm. For the homodyne CW system, the homodyne oscillations of the receiver current ( $I_{Rx}$ ) is proportional to the optical path length difference between the received terahertz field and the laser signal at the receiver. It is expressed as [2]

$$I_{Rx} \sim E_{THz}^0 \cos \left( 2\pi f \frac{\Delta d_{opt}}{c_0} \right), \quad (2)$$

where  $E_{THz}^0$  is the (frequency-dependent) received terahertz field magnitude,  $\Delta d_{opt}$  is the aforementioned optical path length difference,  $f$  is the terahertz frequency and  $c_0$  is the speed of light in vacuum. For example, if the optical path from the DFB-lasers to the transmitter and receiver are identical,  $\Delta d_{opt}$  is given by the free-space THz path between the transmitter and the receiver. This relative optical path length difference can be calculated from the inverse Fourier transform



**Fig. 2.** Equivalent time-domain pulses corresponding to simulated 200 GHz frequency sweeps. The crosses on the plots show exemplary measurement data-points without zero-padding. Zero-padded transforms (red and blue curves) increase temporal and spatial resolution of the IFT, as visible in the inset, where the two peaks are distinguishable from one-another.

(IFT) of Eq. (2), where a peak is visible at a time delay of  $\Delta d_{opt}/c_0$ . For an infinite frequency scan, the peak would resemble a *Lorentzian* function due to the usual roll-off of the receiver current [6]. The finite frequency scan of width  $F_{scan}$  can be understood as a product of the infinite frequency scan with a *rect* function. As the Fourier transform of a *rect* is a *sinc*, the *Lorentzian* peak broadens in the time domain due to its convolution with the *sinc*, where the FWHM of the *sinc* is  $\approx 2\pi/(2.24 \cdot F_{scan})$  [7]. When the surface-structured dielectric sample is subsequently inserted in the THz path, the induced additional phase change at the receiver can be recorded and mapped back to the optical thickness of the substrate, and thus an image of the surface structured sample is reconstructed from estimated thicknesses for each pixel. In essence, we determine the varying optical thickness of the sample using the time of flight information, commonly employed in pulsed [8] or highly broadband THz CW systems [4]. A key feature in this regard is that the peak shape never changes for a lossless material: it is always a convolution between a *Lorentzian-like* function and a *sinc*-function, of which we find the global maximum in order to determine the delay. Even for slightly lossy materials, the peak shape will not noticeably change.

## II. METHODOLOGY AND RESULTS

The Fourier transformed temporal resolution of a frequency bandwidth of 200 GHz is 5 ps, corresponding to an optical thickness resolution of 1.5 mm. To record smaller thickness changes, a frequency scan over a larger bandwidth is necessary, which is constrained by the operational bandwidth of THz system and the measurement time. With some previous knowledge, however, the Fourier limit can be breached. As the shape of the signal, namely the previously discussed convolution of the *Lorentzian-like* peak with a *sinc* function determined by the window size, is known and does not or only slightly change under introduction of a sample, we can determine its peak position in the time domain very precisely by several means: i) fitting the time domain data with a peak function, e.g. a *sinc*, ii) artificially increasing the time domain resolution by zero padding such that the distance of the points is a fraction of the sample height to be resolved, or iii) both at a time. In all three cases, more accurate thickness estimates can

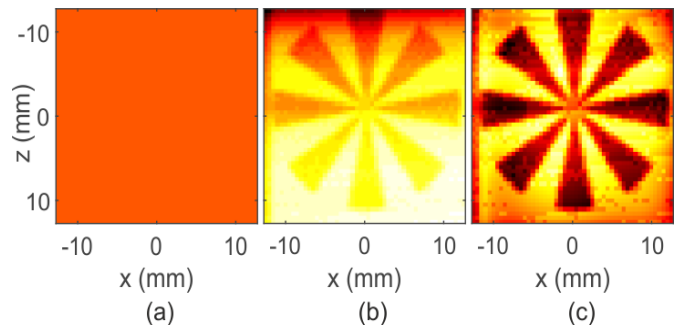


**Fig. 3.** The series of figures show images of a 10  $\mu\text{m}$  deep Siemens star etched into a 520  $\mu\text{m}$  thick HR-Si wafer. Figure (a) image extracted from the time domain trace using a peak search algorithm without any zero-padding. (b) shows the image enhancement by increasing the delay resolution by a factor of 50 by zero-padding of the scan data. Figure (c) image-processed version of (b).

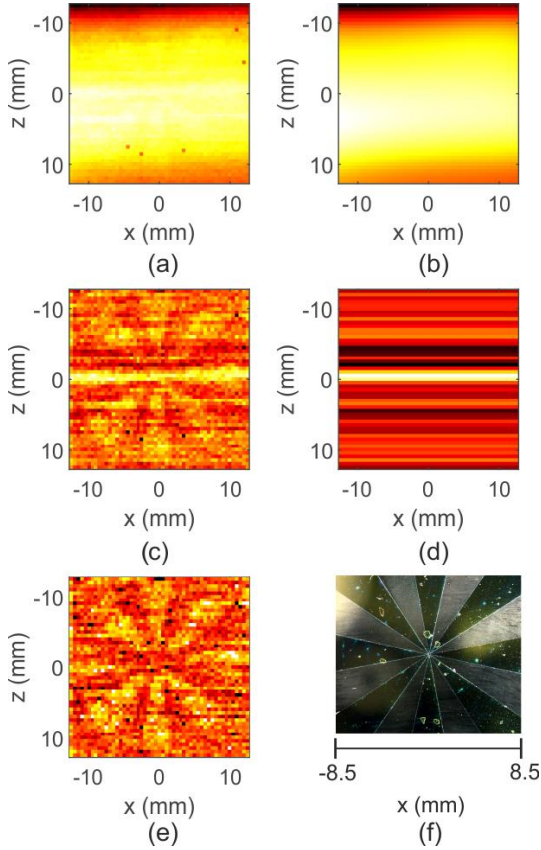
be obtained with smaller scan windows, simplifying the setup, requirements on source and receiver bandwidth as well as offering a reduction of measurement time.

Fig. 2 shows two simulated overlapping equivalent time-domain pulses calculated from two 200 GHz frequency sweeps between 600 GHz and 800 GHz with a 5  $\mu\text{m}$  difference in optical path length/thickness. The crosses show the IFT data points of the 200 GHz sweep. The difference in optical distances travelled by pulses are indistinguishable from this low number of data points without any post-processing. The blue and red plots are obtained by zero padding the 200 GHz scan by an order of 1000, so that it emulates a 200 THz scan, and consequently, the increased spatial resolution to 1.5  $\mu\text{m}$  allows identification the distinct maxima of these two peaks using a simple maxima locator algorithm.

Fig. 3 shows an example image of a 10  $\mu\text{m}$  Siemens star ( $d_{opt} \approx 34 \mu\text{m}$ ) etched into a 520  $\mu\text{m}$  thick highly-resistive silicon (HR-Si) wafer. Fig. 1(a) has the usual optical thickness resolution of 1.5 mm and hence, the Siemens star is not visible. In Fig. 1(b) the frequency scan is elongated by a factor of 50 using zero-padding. The resolution of the corresponding IFT reduces to 30  $\mu\text{m}$  and the relative thickness difference of the HR-Si wafer and etched star becomes discernible. Over the whole measurement time, the frequency of the lasers drift. According to Eq. (2) a frequency drift alters the phase similar to a thickness change. The drift during the whole measurement corresponds to an equivalent thickness change of  $\approx 600 \mu\text{m}$ . This overall frequency drift is approximately linear and can be easily calibrated out by post-processing techniques, which we discuss later in this work. Fig. 3(c) shows the image in Fig. 3(b) with enhanced clarity, evaluated employing such post-processing techniques.

To test the limits of this zero-padding enhanced thickness resolution technique, we further image two HR-Si samples with silicon nitride of thicknesses of 240 nm (SS240) and 350 nm (SS350) (corresponding to optical thicknesses of 490 and 714 nm [2], respectively) deposited atop using chemical vapour deposition. Zero-padding of order 8000 and 2000 are used, respectively, to reconstruct the images of SS240 and SS350. Additional image extraction and enhancement steps are necessary to evaluate these nanometric structures for two reasons. Firstly, the thickness of polished wafer is not uniform throughout and has a surface warping of about 4 – 5  $\mu\text{m}$  [2]. This, along with the overall frequency drift of the lasers,

overshadows the Siemens star, which is orders of magnitude thinner. Secondly, the frequency of the DFB lasers also drifts stochastically during the raster scan of the sample changing the



**Fig. 4.** (a)-(e) show the image processing steps of SS350. (f) shows the corresponding optical micrograph.

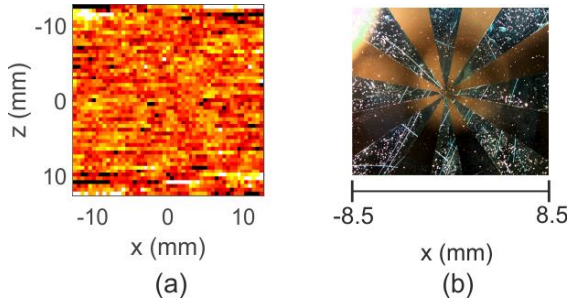


**Fig. 5.** (a) shows the imaged SS240, where the Siemens star is barely visible. (b) shows the optical micrograph of SS240.

measured phase, and consequently, the extracted  $\Delta d_{opt}$ , causing stripes along the scan direction. The error induced by the former is larger than the one induced by the latter and hence, is corrected from the estimated sample thicknesses before compensating for the errors induced by the localised stochastic laser drifts.

Fig. 4 shows the detailed image extraction process for such nanometric structures. The height estimations for SS350 using zero-padding followed by peak-finding of the equivalent time-domain pulse are plotted in Fig. 4(a) as functions of the scanning distances in horizontal ( $x$ ) and vertical ( $z$ ) axes. The star is not yet visible and is hidden under the warping of the host

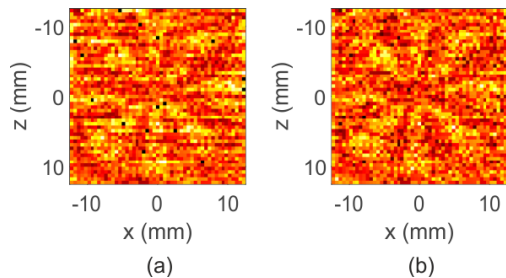
wafer surface. We then calculate the warping plane of the host wafer by calculating a fifth order plane representing the localised 2-D mean of Fig. 4(a) as functions of  $x$  and  $z$ , as shown in Fig. 4(b). The warping plane is then subtracted from Fig. 4(a) to obtain Fig. 4(c). The SS350 structure becomes discernible but is still affected by apparent horizontal localised noise. These horizontal artefacts arise due to the stochastic laser drifts during the raster scan. To reduce these artefacts, we calculate the mean for each horizontal line scan (c.f. Fig. 4(d)) and subtract it from Fig. 4(c) to obtain Fig. 4(e). With additional contrast enhancement, the SS350 structure becomes clearly visible. For comparison, an optical micrograph of SS350 is added in Fig. 4(g). Using the same procedure, we also imaged SS240 as shown in Fig. 5(a). The star is barely visible as the laser drifts could not be adequately removed. Its optical micrograph is shown in Fig. 5(b). An important limiting factor for the imaging technique is, thus, the drifts of the DFB lasers.

TABLE 1: List of processing times taken for different sets of data evaluation techniques for the 350 nm sample, calculated using a zero-padding factor of 2000 and a total pixel count of 2601.

Measurement cases	Processed data length	Time (s)
No down-sampling	8002000	457.98
No down-sampling, (nearest power of 2)	8388608	365.63
10x down-sampled	800200	41.79
10x down-sampled, (nearest power of 2)	1048576	42.83
Fabry-Pérot Estimation [2]	4001	145.82

Higher order IFTs require high processing times and computational effort. The calculations shown in this work are done using “ifft” function of Matlab<sup>TM</sup> on the 64-bit Windows 10 desktop with 32 GB of internal RAM and a 4-Core Intel<sup>®</sup> Core<sup>™</sup> i7-7700 CPU. Table 1 lists the calculated processing times for various height estimation procedures of the SS240 sample. The employed 2000-order zero-padded thickness evaluation shown in Fig. 4(e) needs  $\approx 8$  mins, where  $51 \times 51$  pixels are processed with  $\sim 8$  million data-points per pixel. As per Matlab<sup>TM</sup> documentation, IFTs can be conducted with the zero-padded data length increased to the nearest power of two to reduce the computational effort. The evaluation time in this case reduces by  $\approx 2$  mins, even though the total number of evaluated samples increases. Furthermore, the only relevant data point of the equivalent time-domain pulse for thickness determination is the position of its maxima caused by the homodyne fringes. This allows to down-sample the frequency scan before employing IFT in order to decrease the computational time significantly. A 10-factor down-sampling of the frequency sweep reduces the evaluation time to  $\approx 42$  s, without any significant loss of image quality. In comparison, thickness estimation using a Fabry-Pérot phase fitting algorithm [2] takes  $\sim 2.5$  mins to compute the  $51 \times 51$  pixels of the scanned image. We note here that a low-pass filter is employed before down-sampling for anti-aliasing.

As the periodicity of the homodyne fringes in the detector current determines  $\Delta d_{opt}$  as shown in eqn. (2), theoretically,



**Fig. 6.** (a) and (b) show SS350 imaged with a scanning bandwidth of 50 and 10 GHz respectively.

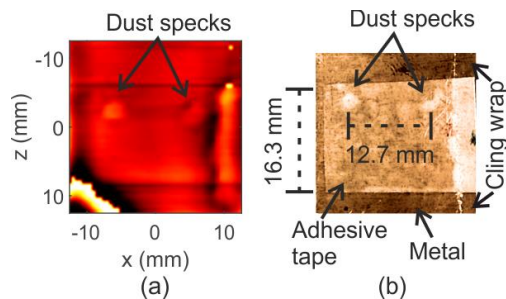


**Fig. 7.** (a) shows a THz image of the optical micrograph shown in (b). The image shows an adhesive tape stuck on a metal reflector where tape outlines and small dust specks under it are visible in THz image.

smaller bandwidth frequency scans can also be used. Fig. 6(a) and (b) are two image reconstructions of SS350 using 50 and 10 GHz frequency scans respectively, centred at 750 GHz, with a zero-padding factor of 2000. The image quality obviously deteriorates, but the stellar pattern is distinguishable from the background noise.

Zero-padding does not add additional information in the equivalent time domain signal. As a result, zero-padded IFT cannot distinguish between the reflections from the multiple surfaces of very thin multi-layered samples, if they are not distinguishable in the non-zero-padded IFT. The optical thicknesses of SS350 and SS240 are, thus, the mean thickness of the HR-Si substrate with and without silicon nitride depositions. However, approximate deposition thicknesses can be estimated from accurate knowledge of the host-wafer thickness and refractive index of the deposited layer.

The demonstrated imaging technique is also applicable for thin films as it measures the absolute change in THz path. We are, indeed, able to visualize a single layer of adhesive-tape (PVC,  $d_{opt} \approx 60 \mu\text{m}$ ) employing this technique as shown in Fig. 6. The Cling wrap layer (PVC,  $d_{opt} \approx 15 \mu\text{m}$ ) at the top-right corner of Fig. 6(a) is also visible on closer inspection. The images shown in this work are solely generated deterministically from the homodyne phase information of the CW measurement system without any high end, computationally expensive data evaluation techniques, such as neural networks or similar [9].

### III. SUMMARY AND OUTLOOK

In summary, we demonstrated an imaging technique by measuring the time-of-flight data through a sample acquired from a 200 GHz frequency scan, where the time resolution is enhanced by zero-padding. We successfully imaged nanometric depositions on HR-Si wafer and thin-films using a bandwidth of 200 GHz between 0.6 – 0.8 THz. The demonstrated

imaging technique circumvents three hurdles of our previous imaging proposition using Fabry-Pérot fitting [2]. Firstly, the image quality is made independent of the minimal sample thickness as multiple Fabry-Pérot oscillation periods are no longer required for data-fitting. Secondly, the data evaluation is faster for structures with thicknesses above a few microns, and comparable for nanometric structures if additional down-sampling is employed. Finally, the maxima-locator technique is not influenced by the measurement noise, given the homodyne fringes are discernible in the frequency sweeps.

This technique is, however, limited to single layered samples and has a worse depth resolution compared to Fabry-Pérot based estimations [2], which in this demonstrated work is  $d_{opt} \approx 500 \text{ nm}$ , i.e. about an order of magnitude worse. Furthermore, unlike Fabry-Pérot based imaging [2], the individual pixel estimates are not independent of the overall frequency drift of the DFB lasers. These laser drifts add additional noise to the image. The deterministic part of the noise, i.e., the gradual changes in the laser frequency, can be calibrated out but the stochastic components cannot be easily removed. Putting aside the increased computational effort for thinner samples, the DFB laser-drifts, thus, impose an absolute limitation on the minimum thickness that can be imaged.

### ACKNOWLEDGEMENTS

We acknowledge the ERC for funding the starting grant PhoT-Lyze GA-No 713780, Dr. Irina Harder and the Group for Nanofabrication TDSU1 from the Max Planck Institute for the Science of Light, Erlangen for her expertise on the D-RIE process, along with providing access to the MPL cleanroom and dry etching facilities. We would also like to thank Alonso Ingar Romero and Korhan Cakir for their assistance in this work.

### REFERENCES

- [1] G. Valušis, A. *et al.*, "Roadmap of Terahertz Imaging 2021," *Sensors* **21**, 4092 (2021)
- [2] Ingar Romero, A., *et al.* Visualizing nanometric structures with sub-millimeter waves. *Nat Commun* **12**, 7091 (2021).
- [3] Born, M., *et al.* Elements of the theory of interference and interferometers, *Principles of Optics: Electromagnetic Theory of Propagation, Interference and Diffraction of Light*, Cambridge University Press (1999).
- [4] Liebermeister, L., *et al.* Terahertz Multilayer Thickness Measurements: Comparison of Optoelectronic Time and Frequency Domain Systems. *J Infrared Milli Terahz Waves* **42**, 1153–1167 (2021).
- [5] A.D.J. Fernandez Olvera, *et al.*, Continuous-wave 1550 nm operated terahertz system using ErAs:In(Al)GaAs photo-conductors with 52 dB dynamic range at 1 THz, *Opt. Express* **25**, 29492-29500 (2017).
- [6] S. Preu, *et al.*, "Tunable, continuous-wave Terahertz photomixer sources and applications", *Journal of Applied Physics* **109**, 061301 (2011)
- [7] S. E. Tavares, "A Comparison of Integration and Low-Pass Filtering," in *IEEE Transactions on Instrumentation and Measurement* **15**, 33-38 (1966)
- [8] Jun Takayanagi, *et al.*, "High-resolution time-of-flight terahertz tomography using a femtosecond fiber laser," *Opt. Express* **17**, 7533-7539 (2009)
- [9] Schreiner, N. S., *et al.* Multilayer Thickness Measurements below the Rayleigh Limit Using FMCW Millimeter and Terahertz Waves. *Sensors* **19**, 3910 (2019)

©2022 IEEE. Personal use of this material is permitted. Permission from IEEE must be obtained for all other uses, in any current or future media, including reprinting/republishing this material for advertising or promotional purposes, creating new collective works, for resale or redistribution to servers or lists, or reuse of any copyrighted component of this work in other works.

Published article: A. K. Mukherjee and S. Preu, "Emulating a broadband frequency sweep for Terahertz thin-film imaging," *2022 47th International Conference on Infrared, Millimeter and Terahertz Waves (IRMMW-THz)*, 2022, pp. 1-4, doi: 10.1109/IRMMW-THz50927.2022.9895797.

Urheberrechtlich geschützt / In Copyright